

Experimental detection of microscopic environments using thermodynamic observables

Raam Uzdin¹ and Nadav Katz²

¹*Fritz Haber Research Center for Molecular Dynamics, Institute of Chemistry,
The Hebrew University of Jerusalem, Jerusalem 9190401, Israel and*

²*Racah Institute of Physics, The Hebrew University of Jerusalem, Jerusalem 9190401, Israel*

Macroscopic objects are subjected to the three laws of thermodynamics. However various modern theories predict that the second law has many companion constraints that manifest in microscopic and quantum systems. We use the IBM superconducting quantum processors to experimentally test the predictive power of these constraints compared to the second law and to each other. Our experimental demonstration is based on an operational test where a system is coupled to a small environment that creates a heat leak. The goal is to detect the heat leak using only measurements on the system. Since the system is not isolated some of the constraints may be violated. Constraints that are not violated, are weaker than ones that do. In our example, we find that the global passivity constraints are stronger than those of resources theory and the standard second law of thermodynamics. Yet they are weaker than the passivity deformation constraints. Finally, it is shown that in the present setup heat leak detection based on fluctuation theorems is considerably more difficult to do compared to a simple majorization test that has the same detection capabilities.

I. HEAT LEAK DETECTION AS A BENCHMARK FOR THERMODYNAMIC THEORIES

In recent years several different thermodynamic theoretical frameworks (frameworks, hereafter) for microscopic and/or quantum systems have been formulated and investigated. These frameworks are stochastic thermodynamics [1, 2], thermodynamic resource theory [3–7], global passivity [8], and the more established frameworks of quantum information (in thermodynamic context) [9–13], and the Master equations of open quantum system (weak coupling limit) [14]. Quantum thermodynamics binds together the thermodynamic frameworks that are consistent with quantum dynamics [11, 15–17] (see also the recent collection [13]).

All these frameworks set bounds on the allowed dynamics without knowing the details of the dynamics itself (i.e. the external driving and the coupling protocols). In stochastic thermodynamics, fluctuation theorems [1, 2, 18] provide an equality for the average of the exponent of the work. A version that is more suitable to heat machines and to the present paper has been derived in [19]. Thermodynamic resource theory provides a continuous family of constraints [4] on a specific type of interactions called thermal operations. One of these constraints is the free energy form of the second law for a single thermal environment. From a quantum information perspective, a quantum microscopic version of the second law has been derived [9, 12, 13, 20]. Within the framework of open quantum systems and the quantum Master equations, there is a constraint on the rate of entropy production [14]. Finally, a thermodynamic framework based on the concept of global passivity [8] provides a continuous family of constraints as well (one of them is the second law). Yet, in contrast to resource theory, these

constraints involve only expectation values of observables quantities.

Which framework will prevail in which scenario? Which one is better suited for the experimental challenges in the near and distant future? Apart from their different level of utility, some frameworks may pose more strict restrictions on the dynamics compared to others. One of the main difficulties in comparing completely different frameworks is that they deal with different quantities. In some frameworks these quantities are not even observables (in the sense of expectation value of Hermitian operators). In other frameworks, like stochastic thermodynamics, the prediction is on the statistics of “trajectories” and not on the change in some observable (e.g. energy) or an information measure (for example, entropy).

To tackle this problem, we suggest a framework-independent operational test. For these frameworks to be valid in a given setup, the setup has to be sufficiently isolated from the rest of the world. Here, a “setup” refers to all the elements of interests, such as thermal environments, and the heat machines that exploit them. In our scheme, we tamper with this isolation in a controlled way and check which framework “fails” first. In the present context a failure is a good thing. A framework that fails for weaker tampering is more restrictive than others that do not fail.

In the present experiment two qubits (‘c’ and ‘h’) constitute the system and one qubit (‘e’) act as an unaccounted environment that violates the isolation of the c-h system. We test different thermodynamic inequalities *in the two-qubit system* and check which ones are violated due to the presence of the environment qubit ‘e’. As a quick preview, we refer the reader to Fig. 1a where we compare a continuous family of inequalities from the framework of global passivity to the standard second law.

Each α value corresponds to a different inequality which we apply to the c-h system. In particular, $\alpha = 1$ corresponds to the standard second law in microscopic setups for two thermal environments (as described later in detail). In isolated setups the change in the expectation value of the operator B^α (described later) should be positive. The evolution is carried on the IBM quantum processors [21] and the circuit that describes the evolution appears in Fig. 2b). As shown in Fig. 1a for $\alpha = 1$ $\Delta \langle B \rangle > 0$ which means that the second law is incapable of detecting the interaction with the qubit 'e'. Yet, we observe that for some other values of α the global passivity inequality satisfy $\Delta \langle B^\alpha \rangle < 0$ which indicates that the system is not isolated. Thus, in this example, global passivity is more sensitive and more restrictive than the second law. Whether this is always the case or not is an open question, and yet from analyticity, it is unlikely that $\alpha = 1$ will be the only point where $\Delta \langle B^\alpha \rangle < 0$ while for $\alpha \neq 1$ $\Delta \langle B^\alpha \rangle > 0$. The inset in 1a shows that if the interaction with qubit 'e' is removed so that the c-h system is isolated from the rest of the world (for the duration of the experiment) then $\Delta \langle B^\alpha \rangle \geq 0$ holds for all α .

In this paper we carry out a study of a specific setup implemented in the IBM superconducting quantum processors. We show that the predictions of global passivity are experimentally relevant and that they provide better predictions than the second law and resource theory. Next, we explore the prediction of the passivity deformation framework and find that it outperforms the global passivity inequalities. In addition, we discuss why fluctuation theorem are not useful for heat leak detection in the present setup. Finally, it is shown numerically that global passivity detection is valid for larger setups as well.

II. THE QUANTUM CIRCUIT AND ITS REALIZATION

The experimental scheme in Fig 2a, has three parts: the initialization circuit (a), the evolution circuit (a), and the detectors. Each part requires special attention.

A. The circuit of the quantum evolution

As explained earlier, our setup consists of three qubits: two qubits for the system and one for generating the heat leak. Hence, the two-spin c-h system constitutes an open system that does not evolve unitarily. The IBM machines follow the circuit paradigm so the interactions must be constructed from a given set of quantum gates. To avoid accumulated gate errors we choose the minimal number of gates that can show non-trivial heat leak detection. We emphasize that the actual evolution is of no particular interest on its own - we only care about detecting

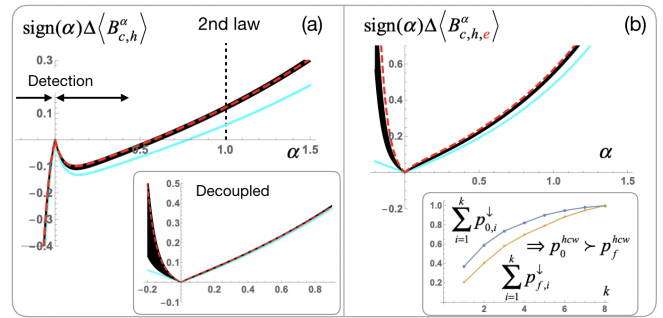


Figure 1. In plots a & b, negative values correspond to heat leak detection. The black lines corresponds to the experimental results (the width is the uncertainty), the red lines are the theory prediction with the calibrated unitary, and the cyan lines stand for the ideal error-free circuit. (a) In this experiment, the second law ($\alpha = 1$) cannot detect the heat leak while the global passivity inequalities ($\alpha \neq 1$) can detect it some values of α . For comparison, the inset shows the results without the heat leak. (b) When applied to the whole three-qubit setup the global passivity yields positive values as expected (no heat leak). The inset shows a test of majorization relations which unequivocally validates the validity of the global passivity inequality to this setup (e.g. it confirms that the T1 decay effects can be safely ignored).

the heat leak and not about implementing a specific algorithm. In fact, the heat leak detection challenge could be formulated with a degree of freedom to choose any circuit between c and h. Nonetheless, here we study a specific circuit. To carry out the evolution, we send the processor the three-CNOT circuit shown in Fig. 2b. On top of that, we have additional gates that prepare the thermal initial condition as described in the next section. The observables we use must include only qubits 'c' and 'h'. Yet, for calibrations and validation purposes, we measure all three qubits.

B. Creation of the initial conditions

By default, in the IBM processors all the qubits are initialized in the ground state. With the present software interface to the processors, we were unable to directly prepare the desired initial distribution. Thus, to create a thermal mixed state, we first rotate the initial ground state of the qubit by an angle θ in the x-z plane of the Bloch sphere. This angle is chosen so that the projection on the z axis fits the thermal population we wish to achieve. While some circuits may be insensitive to this initial local phase, we prefer to be more general and average out this phase in the initial conditions. By running the θ and $-\theta$ preparations equal amount of times, a diagonal ensemble is achieved. For a three-qubit setup 2^3 coherent preparations are needed to form a fully diagonal ensemble: $\{\pm\theta_c, \pm\theta_h, \pm\theta_e\}$.

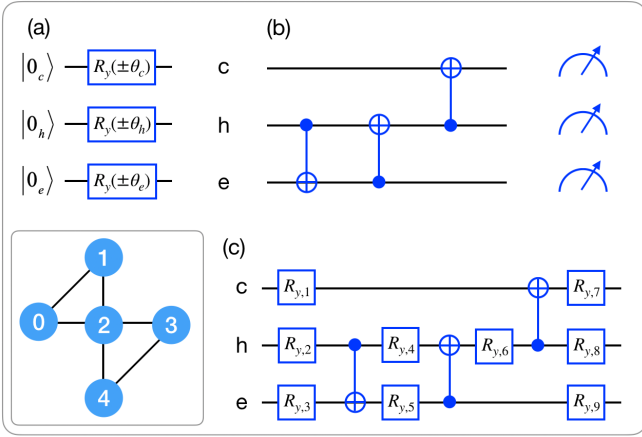


Figure 2. The experiment was performed on the 'Tenerife' IBM superconducting quantum processor. (a) The first part of the circuit creates the thermal initial conditions. (b) The second of the circuit implements the evolution including the heat leak. (c) The circuit used for the unitary calibration.

C. Detector noise calibration

At the end of the circuit, the qubits are measured in the $\{|0\rangle, |1\rangle\}$ basis which we identify with the energy basis - the basis of the initial diagonal ensemble. In this setup, the detectors that carry out these measurements are far from being perfect. For example, in the Tenerife processor, the error rate is $0.07 - 0.2$, that is 7-20% of the times there will be a readout error. The error varies from one qubit to another and this affects which three qubits out of the five we choose to work with. For the Yorktown processor, the readout error is $\sim 0.015 - 0.045$ (this updated data was taken from the IBM quantum experience website at the time of the experiment). However, the Yorktown processor has higher gate errors compare to the Tenerife processor as discussed in the next section.

Fortunately, the detector errors can be mapped and taken into account. To do so we first measure the detector noise without a circuit and build a detector matrix M that translates the real probabilities to the ones the detectors provide. Once M is available we can use its inverse to remove the effect of the detector. This should be done with care as in some special cases small negative probability might appear. Yet we verify that this never happens in our experiment. To check the validity of the M^{-1} detector compensation, we run a set of measurements directly after the initialization circuit and calculate the measured angle. The data in Appendix II demonstrates that this procedure works very well.

D. Coping with significant gate errors

The gate errors in the processors we had access to is substantial. In the Tenerife machine the CNOT's we

have used have error rates of $\sim 2.5 - 3\%$, and in the Yorktown processor it is $\sim 3.5 - 4.5\%$. As a result, the transformation of the population in the density matrix $\text{diag}(\rho_0) \rightarrow \text{diag}(\rho_f)$ is different from that expected from the ideal transfer matrix T_{ideal} generated by the three CNOT's circuit in Fig. 2b. Importantly, the errors in the final result can be much more than 2 - 5%. The main reason is that we look at *changes* with respect to the initial state. Depending on the dynamics and the initial conditions these changes, or at least the changes that contain the information on the heat leak, might be very small. Consequently, a few percent of error can be a major problem.

To quantify the difference between the experimental circuit and the ideal circuit, the evolution operator itself has to be measured (i.e. process tomography). However, since the measurements in this experiment are carried out in the energy basis, there is access only to the population transfer matrix that connects the initial populations p_0 to the final one p_f , i.e. $p_f = T p_0$. T_{ideal} is obtained by applying the unitary that describes the ideal circuit to the computational basis. T_{exp} is measured by using the computational basis as input to the circuit and recording the response for each basis element. In principle, T_{exp} should be compared to T_{ideal} , but T_{exp} contains the detector errors as well, so the proper comparison is $M T_{\text{ideal}}$ vs. T_{exp} . In the Yorktown experiment, we find that L2 norm is $\|T_{\text{exp}} - M T_{\text{ideal}}\|_2 = 0.635$ ($\|T_{\text{exp}} - M T_{\text{ideal}}\|_2 / \|T_{\text{exp}}\|_2 = 0.32$) and in the Tenerife processor it is 0.135 ($\|T_{\text{exp}} - M T_{\text{ideal}}\|_2 / \|T_{\text{exp}}\|_2 = 0.077$) which reflects its lower error rate with respect to the Yorktown machine. The difference between the ideal circuit and the experimental one is illustrated, for example, in Fig. 1a. The black curve depicts the experimental results, and the cyan curve is the prediction of the ideal circuit.

A key observation which applies to thermodynamic experiments of the present type (in contrast to heat machines and quantum computing experiments) is that the exact unitary that takes place is not really important as long as the effect of interest (i.e. heat leak detection) is observed. With this in mind, we can look for other unitaries U' that lead to $M T(U')$ that is closer to T_{exp} . Finding the unitary that mimics this transfer function is not a trivial task. Our approach is motivated by the fact that CNOT gates in the IBM machines are based on the cross phase technology. We assume that some of the single qubit gates inside the CNOT are not perfectly implemented and we add R_y rotations to correct it as depicted in Fig. 2c. Each R_y may have a different rotation angle. Next, we numerically search for a minimum of the error function $\text{err}_{\text{fix}} = \|M T(U_{\text{fix}}) - T_{\text{exp}}\|_2$ where U_{fix} is the unitary given by the circuit in Fig. 2c. Although the parameters we obtain are not guaranteed to be a global minimum they significantly reduce the error. In the Yorktown machine the initial L2 error 0.635 is

dramatically reduced to 0.073 (relative error reduces to 0.038). In the Tenerife machine the initial L2 error 0.206 is significantly reduced to 0.032 (relative error reduces to 0.0183). Although the improvement in Yorktown is larger (factor of 8.6 vs. 4.2 in Tenerife), the Tenerife processor starts with a lower gate error rate, and therefore still retains an advantage over Yorktown after this unitary calibration procedure. This should be taken with a pinch of salt as it is not guaranteed that we found a global minimum in the optimization.

Indeed, we use here a numerical fit to do a post mortem calibration. This, however, should be put in the right context: 1) we do not change the experimental data used for the thermodynamic isolation tests. We only find a better description of the evolution operator for the numerical simulation. 2) we do not modify thermodynamic constraints in any way or try to make them work better. 3) Most importantly, it is possible to take a *circuit-agnostic approach* and treat the circuit as a black box. Our goal is only to measure the inputs and outputs of the c-h system and check if the heat leak is detectable using different thermodynamic frameworks. Thus, this unitary calibration mainly provides reassurance that the evolution of the three qubit is close to unitary evolution albeit different from the planned one.

We point out that the observed majorization relation discussed later is already sufficient to confirm that the various frameworks (excluding resource theory) are applicable to this setup. This confirmation uses only the measured data and has nothing to do with the unitary calibration procedure. The unitary calibration is done once for each processor during the experiment.

III. GLOBAL PASSIVITY

In [8] it was shown that in a setup where all the elements are initially uncorrelated and start in some thermal Gibbs state

$$\rho_0^{tot} = e^{-\beta_1 H_1} \otimes e^{-\beta_2 H_2} \otimes \dots$$

where β_i is the initial inverse temperature, it holds that for any real [22] α

$$\text{sign}(\alpha) \Delta \langle B^\alpha \rangle \geq 0 \quad (1)$$

$$B = \sum_k \beta_k H_k - \min(\sum_k \beta_k H_k) I \quad (2)$$

for any unitary evolution $\rho_f^{tot} = U \rho_0^{tot} U^\dagger$ (in the theoretical framework the use of the population transfer matrix as in Sec. IID is more cumbersome). The subtraction of $\min(\sum_k \beta_k H_k)$ times the identity matrix I , makes sure that B is a positive operator. Moreover, even if B happens to be positive this shift provides better detection performance compare to the unshifted operator. From

linearity in the density matrix it follows that (1) holds for any mixture of unitaries:

$$\begin{aligned} \rho_0^{tot} &= \sum f_k U_k \rho_0^{tot} U_k^\dagger \\ \sum f_k &= 1 \end{aligned} \quad (3)$$

where f_k is the probability that a unitary U_k takes place.

For $\alpha = 1$, (1) reduces to the entropy-free form [13] of the second law

$$\sum \beta_k q_k \geq 0, \quad (4)$$

where $q_k \doteq \Delta \langle H_k \rangle$ which is often referred to as heat [13], is the change in the energy of microbath k . A microbath [13] is an environment (potentially a very small one) whose *initial* state is thermal. In contrast to macroscopic baths, a microbath is easily taken out of equilibrium once interacting with other elements.

In our case, the ideal circuit in Fig. 1b generates a unitary evolution for the three-qubit setup. However, the reduced dynamics of the c-h subsystem is a Kraus Map (ideally) and not a unitary or a mixture of unitaries. This is easy to see since a fully mixed state in c-h is not a fixed point of the dynamics (non-unital map). More precisely the evolution of the c-h subsystem is given by

$$\rho_f^{ch} = \text{tr}_e[U \rho_0^{ch} \otimes \rho_0^e U^\dagger] \quad (5)$$

As a result, it is not guaranteed anymore that (1) holds. By negation, we can conclude that if $\Delta \langle B_{c,h}^\alpha \rangle < 0$ is observed, the evolution is not unitary and the setup is not isolated. The most famous example where external interaction leads to an *apparent* violation of a thermodynamic principle, is the Maxwell demon scenario where a feedback operation (i.e. not an evolution of the form (3)) leads to $\sum \beta_k q_k < 0$ which in the Maxwell demon setup implies an energy flow from cold to hot without investing work. Crucially, we are interested in cases where $\sum \beta_k q_k \geq 0$ is satisfied although the evolution is not a mixture of unitaries. That is, the second law is not restrictive enough for detecting the lack of isolation. Autonomous demons (without measurement) can be implemented using an additional zero temperature bath. Thus, feedback and demons can be formally viewed as an interaction with another bath i.e. a heat leak.

IV. EXPERIMENTAL RESULTS

A. The protocol of the experiment

The experiment is composed of 20 executions of the same protocol where each execution contains both measurement of M and T_{exp} and ensembles of pure initial conditions that together form the desired diagonal initial condition. One diagonal ensemble is used for evaluating

$\langle B^\alpha \rangle$ right after preparing the initial conditions, and the other diagonal ensemble is used for measuring $\langle B^\alpha \rangle$ at the end of the circuit. The rotation angle we chose are $\theta_c = \theta_e = \pm \frac{\pi}{4}$ and $\theta_h = \pm \frac{4}{10}\pi$. A $\pi/4$ rotation corresponds to $\beta\omega \simeq 1.75$ and $\frac{4}{10}\pi$ to $\beta\omega \simeq 0.63$. T_{exp} is used only for the unitary calibration in the numerical simulation, and it is not used in the experimental detection procedure.

In Fig. 1a. the black curve shows the experimental result, and its width corresponds to 99% statistical confidence interval (see Appendix II). The cyan line stands for the numerical simulation using the uncalibrated circuit 2b, and the dashed-red line shows the result of the calibrated circuit 2c. For negative α and for $0 < \alpha \leq \sim 0.35$ a negative change in $\langle B_{c,h}^\alpha \rangle$ is observed, and we conclude that the c-h system is not isolated. That is, the heat leak is detected. Crucially, in this example for $\alpha = 1$ we find $\Delta \langle B_{c,h} \rangle \geq 0$, i.e. the second law (4) cannot detect the heat leak. For comparison, in the inset of Fig. 1a we plot the same quantities when the environment qubit 'e' is disconnected (i.e. without the first two CNOT gates). As expected, since there is no heat leak $\Delta \langle B_{c,h}^\alpha \rangle \geq 0$ is observed for all α values.

Most importantly, in appendix V we show that the global passivity heat leak detection still works when the system size is increased and the environment remains small. Furthermore in Appendix VI it is shown that these result are reproduced on other quantum processors (the 14-qubit Melbourne processor, and the 5-qubit Yorktown processor) despite their higher level of gate errors.

1. Full setup results

Apart from the good agreement between the simulation and the experiment (and the inset in 1a), to exclude that the negative values are due to some artifacts in the c-h system and not due to the heat leak, we check if $\Delta \langle B^\alpha \rangle \geq 0$ holds when applied to the whole c-h-e setup. Fig. 1b shows that indeed $\Delta \langle B_{c,h,e}^\alpha \rangle \geq 0$ as expected from the fact that the three qubits are well isolated (for the time of the experiment which is much shorter than T1). Furthermore, in the inset of 1b we plot the measured cumulative sum of the sorted initial and final probabilities (decreasing order). The fact that the two curves intersect only trivially at the value 1 on the y axis means that p_0^{tot} majorizes p_f^{tot} . Since any majorized distribution can be obtained from its majorizing distribution by a mixture of permutations (doubly stochastic map)[23], global passivity is perfectly valid for this setup. That is, there is mixture of unitaries (3) that reproduces the transformation $p_0^{tot} \rightarrow p_f^{tot}$.

V. HEAT LEAK DETECTION BASED ON OTHER FRAMEWORKS

In what follows we exploit additional thermodynamic frameworks and compare their detection capability to global passivity. In particular, we look at resource theory, passivity deformations, and the relevant integral fluctuation theorem.

A. Resource theory

Resource theory (RT) predicts that under operations called “thermal operation” there is a family of additional inequalities on top of the second law. Thermal operations are interactions with a microbath that conserve the sum of the system energy and the microbath energy. The constraints come from the contractivity of the Rényi divergence under CP maps with a thermal fixed point (i.e. thermal operation) [4, 7]. The constraints take the following form

$$-(D_\alpha^R(p_{f,sys}|p_{\beta,sys}) - D_\alpha^R(p_{0,sys}|p_{\beta,sys})) \geq 0 \quad (6)$$

where $D_\alpha^R = \frac{1}{\alpha-1} \text{tr}[x^{\tilde{\alpha}} y^{1-\tilde{\alpha}}]$ is the Rényi divergence between two vectors x and y , $p_{0(f)}$ are the initial (final) populations in the energy basis and $p_{\beta,sys}$ is the thermal state of the system. See [6] for restrictions on the coherent part of the density matrix. Unfortunately, there are two main problems when trying to apply RT to experiments of the type discussed in the present paper:

1) The theory does not provide predictions on observables but on some nonlinear function of the density matrix as shown in (6). Moreover, these functions do not have the properties of proper information measures (e.g, they are not invariant under permutations or unitary transformation, and they do not always increase when subjected to a unital map).

2) Thermal operations require energy-conserving interaction with the thermal environment. That is, the c-h part of the circuit should not supply or harvest work.

These two generic difficulties in applying resource theory suggest that in its present form the theory is not of very broad applicability to experiments. Nevertheless, for the sake of comparison, these two difficulties can be resolved to some extent in this specific setup. Since RT deals only with the reduced dynamics of one element ('c' or 'h' in the present case), measuring the spin polarization $\langle \sigma_z \rangle$ will fully determine the reduced density matrix of that single spin (given that it is diagonal as in the ideal circuit with thermal initial conditions). To handle the second limitation, we replace the third CNOT in Fig. 2 by an energy-conserving swap operation (all the qubits have the same energy gap) as shown in the inset of Fig. 3.

Unfortunately, running this circuit we encounter several problems. First, in the IBM machines the swap is im-

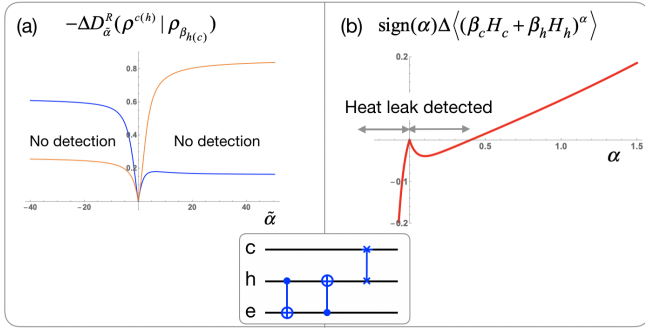


Figure 3. The circuit in the inset is used for checking heat leak detection based on resource theory. (a) Numerically checking the Rényi-divergence-based resource theory inequalities. In blue (orange) curve, 'c' ('h') is treated as the system and 'h'('c') as the environment (microbath). In both cases there is no violation of the resource theory inequalities and the heat leak cannot be detected. Due to the gate errors an experimental realization of the necessary thermal operation was not possible (b) Global passivity test for the same scenario. For $\alpha < 0.4$ the global passivity inequalities clearly detect the heat leak.

plemented via three CNOTs, so the gate error is substantially larger than in the previous circuit. In particular, we see poor energy conservation (10-15% deviation). Furthermore, although this is not a mandatory requirement, the unitary calibration is not as successful in this circuit as it was with a CNOT instead of the SWAP (again due to the larger error).

Nevertheless, for the sake of comparison and the potential future experiments with less noise, in this part of the paper we carry out a numerical simulation without doing the experiment. If we use the same angles (temperatures) in the present circuit we find that global passivity detects the heat leak for any α . To avoid detection by the second law $\alpha = 1$ we set $\theta_e = 0.35$ and keep the other angles as they were. In Fig. 3a we check the validity of (7) in the presence of the heat leak. Here there are two possibilities. We can choose spin 'c' as the system and the ρ_β will be the thermal state of 'c' with the initial temperature of the hot qubit (that dictates the fixed point of 'c'). Alternatively, we can choose 'h' to be the system and 'c' to be the environment. In Fig. 3a we plot both options and find that neither can detect the heat leak. In contrast Fig. 3b, shows that global passivity can easily detect the heat leak for some values of α .

Finally, in appendix III we show analytically a scenario in which resource theory will never be able to detect a heat leak, even though it is detectable by other frameworks.

B. Passivity deformation

Passivity deformation [24] (see Appendix IV), is a new scheme for constructing thermodynamic inequalities in a given setup. Passivity deformation has a few appealing features: 1) It can contain fine-grained or coarse-grained quantities of interest that do not appear in the standard second law and in global passivity. 2) In contrast to the standard second law and global passivity, it provides tight inequalities also in microscopic setups (i.e. microscopic environments). 3) Like global passivity, the passivity deformation framework involves only expectation values so state tomography is never needed. The second feature is of great importance to the present experiment and more generally to thermodynamic isolation tests. The inherent tightness of the passivity deformation bounds implies that passivity deformation may provide superior isolation tests compared to global passivity and the second law.

To illustrate this, we use the same circuit shown in Fig. 2b but with the following initial conditions $\theta_h = 0.5\pi$, $\theta_h = \theta_e = 0.25\pi$. The reason for changing the parameters is that we want to have an example where global passivity cannot detect the heat leak. These new parameters lead to a heat leak that is more difficult to detect. One of the predictions of the passivity deformation framework *for the present setup* (see appendix IV) is remarkably simple: it states that β_c could be replaced by β_h so that the second law in the c-h system $\sum_{k=h,c} \beta_k q_k \geq 0$ turns into:

$$\Delta \langle H_c + H_h \rangle \geq 0,$$

i.e. despite the temperature difference it is not possible to build an engine between c and h (see appendix IV for the derivation). The result in Fig. 4a shows that the global passivity B^α test is incapable of detecting the heat leak. However, Fig. 4b shows that the passivity deformation test $\Delta \langle (H_c + H_h)^\alpha \rangle < 0$ easily detects the heat leak. We conclude that this experimental example illustrates the added value of the passivity deformation framework.

VI. DETECTION BASED ON A FLUCTUATION THEOREM

The c-h system starts in *local* thermal equilibrium (c-h is not in a thermal state) and therefore if the system is isolated the following integral fluctuation theorem [19] holds

$$\langle \langle e^{-\beta_c Q_c - \beta_h Q_h} \rangle \rangle = 1 \quad (7)$$

where $Q_{c(h)}$ is the change in energy in a specific trajectory. A trajectory is obtained by measuring the energy in h and c before and after the circuit is executed. However, the average energy is not evaluated. Instead we

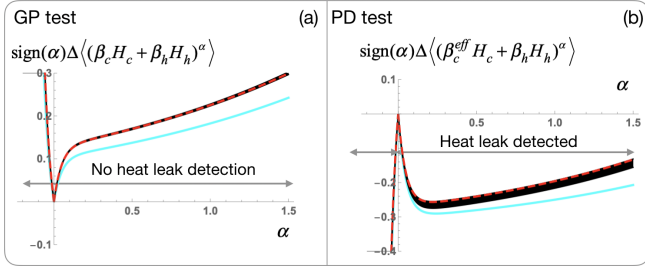


Figure 4. (a) In this experiment (black curves) we set the parameter so that global passivity cannot detect the heat leak for any α . The red curve shows the theory with the calibrated unitary, the cyan line depicts the prediction of the ideal circuit, and the black curve stands for the experimental results where the width indicates the experimental uncertainty. (b) The passivity deformation framework provides tighter inequalities. In this specific case the observable is obtained by replacing β_c by $\beta_c^{eff} = \beta_h$ instead of the physical β_c . As a result, the heat leak is detected as the figure shows. Remarkably even the $\alpha = 1$ inequality detects the heat leak. Yet this time $\alpha = 1$ is not standard second law due to the use of β_c^{eff} .

look at events where some initial realization $\{E_i^c, E_j^h\}$ is mapped to some realization at the end of the evolution $\{E_{i'}^c, E_{j'}^h\}$. In this setup, the set $\{i, j, i', j'\}$ describes a trajectory. The double bracket average stands for averaging over all possible trajectories.

The problem is that in the experiments described above, we have access only to the initial and final distribution. For example, if for some level we observe an increase of population we do not know which levels contributed to this increase - there is no trajectory information in the measurements we have carried out until now. To get access to this information one needs to prepare the setup in a deterministic state (i.e. in some levels i and j) and record the obtained final distribution. To obtain the full trajectory statistics this has to be repeated for all levels. This procedure is fully equivalent to process tomography for the diagonal elements (the transfer function T).

In the present setup, this is possible since we construct the thermal initial condition from pure states but in general, for a given initial distribution such process tomography might not be possible. More importantly, if we allow the use of the full initial and final distributions (without trajectory information) we can simply check the majorization conditions which is a sufficient condition for dynamics of the form (3). Both the fluctuation theorem (7) and the majorization relation require doubly stochastic dynamics to hold. We conclude that although, in principle, fluctuation theorems can be used, they are more difficult to evaluate compared than other alternatives that possess exactly the same heat leak detection capabilities.

VII. CONCLUSION

In this paper, we show the relevance of modern thermodynamic frameworks to small isolated quantum setups. The setup considered in this experiment is the smallest one that enables us to compare the different frameworks via an operational test. Nonetheless, there is no theoretical limitation to implement it to setups that are too big to be solved analytically or numerically e.g. in cold atoms in optical lattices. Despite the large detector noise and the significant gate error we still get a good match between the experiment and the numerical simulation that takes this effect into account.

We use heat leak detection as an operational test and a benchmark for comparing completely different thermodynamic frameworks. The theoretical limits of heat leak detection (i.e. the sensitivity) are still not known and warrant further theoretical and experimental study.

It is crucial that any new detection methodology will be put to an experimental test. Apart from the feasibility of using the bound with the experimental noise and the limits of data collection, an experiment shows the resources needed to evaluate the bounds. As an example, in the present setup work of individual trajectories cannot be directly measured so a process tomography is needed for using bounds based on fluctuation theorems. Such process tomography is much more demanding than directly checking the majorization condition. The high cost of using fluctuation theorems is typical to quantum circuits and not just for the present setup and the specific circuit we used.

We hope that this study will motivate further investigation in other experimental setups such as trapped ions and cold atoms in optical lattices that can potentially explore regimes that are not accessible by the IBM platform we have utilized in the present work.

-
- [1] U. Seifert, Reports on Progress in Physics **75**, 126001 (2012).
 - [2] K. Sekimoto, *Stochastic energetics*, Vol. 799 (Springer, 2010).
 - [3] G. Gour, M. P. Müller, V. Narasimhachar, R. W. Spekkens, and N. Y. Halpern, Physics Reports **583**, 1 (2015).
 - [4] F. Brandão, M. Horodecki, N. Ng, J. Oppenheim, and S. Wehner, Proceedings of the National Academy of Sciences **112**, 3275 (2015).
 - [5] M. Horodecki and J. Oppenheim, Nature communications **4**, 2059 (2013).
 - [6] M. Lostaglio, D. Jennings, and T. Rudolph, Nature communications **6**, 6383 (2015).
 - [7] M. Lostaglio, arXiv preprint arXiv:1807.11549 (2018).
 - [8] R. Uzdin and S. Rahav, Phys. Rev. X **8**, 021064 (2018).
 - [9] A. Peres, *Quantum theory: concepts and methods*, Vol. 57 (Springer Science & Business Media, 2006).

- [10] M. Esposito, K. Lindenberg, and C. Van den Broeck, *New Journal of Physics* **12**, 013013 (2010).
- [11] J. Goold, M. Huber, A. Riera, L. del Rio, and P. Skrzypczyk, *Journal of Physics A: Mathematical and Theoretical* **49**, 143001 (2016).
- [12] T. Sagawa, *Lectures on Quantum Computing, Thermodynamics and Statistical Physics* **8**, 127 (2012).
- [13] R. Uzdin, As a chapter of: F. Binder, L. A. Correa, C. Gogolin, J. Anders, and G. Adesso (eds.), "Thermodynamics in the quantum regime - Recent Progress and Outlook", (Springer International Publishing). arXiv: 1805.02065.
- [14] H.-P. Breuer and F. Petruccione, *Open quantum systems* (Oxford university press, 2002).
- [15] S. Vinjanampathy and J. Anders, *Contemporary Physics* **57**, 545 (2016).
- [16] G. Benenti, G. Casati, K. Saito, and R. S. Whitney, *Physics Reports* **694**, 1 (2017), fundamental aspects of steady-state conversion of heat to work at the nanoscale.
- [17] Z. Merali, *Nature News* **551**, 20 (2017).
- [18] M. Campisi, P. Hänggi, and P. Talkner, *Rev. Mod. Phys.* **83**, 771 (2011).
- [19] M. Campisi, J. Pekola, and R. Fazio, *New Journal of Physics* **17**, 035012 (2015).
- [20] M. Esposito and C. Van den Broeck, *EPL (Europhysics Letters)* **95**, 40004 (2011).
- [21] <https://www.research.ibm.com/ibm/q/technology/experience/>, .
- [22] The $\text{sign}(\alpha)$ was not included in the original paper [8] where α was limited to positive values. In the present form α can be any real number.
- [23] A. W. Marshall, I. Olkin, and B. C. Arnold, *Inequalities: theory of majorization and its applications*, Vol. 143 (Springer, 1979).
- [24] R. Uzdin and S. Rahav, In preparation.

APPENDIX I - DETECTOR NOISE

To evaluate M we chose the input states as the computational basis $\{0_e 0_h 0_c, 0_e 0_h 1_c, 010, 011, \dots\}$ and denote it by v_0, \dots, v_7 . Next, we run the maximum number of runs of the experiments that can be done for a single preparation ("shots") which is 8192 shots. The response of each input state v_i is recorded p_0^D, \dots, p_7^D and the detector matrix M is constructed setting p_i^D as the columns of the matrix M . The measurement of M has statistical fluctuations, so M has to be measured multiple times. Multiple measurements of M are also important for detecting systematic drifts in time of the detector noise.

Table 1 shows the results with and without the M^{-1} detector compensation for the Tenerife and Yorktown processors.

APPENDIX II - LEVEL OF CONFIDENCE CALCULATION

To evaluate the statistical error of our measurements we treat each incoherent ensemble i.e. 8 coherent batches

| Tenerife | Theory | without M^{-1} | with M^{-1} |
|------------|-----------|------------------|---------------|
| θ_e | 0.25π | 0.36137π | 0.25137π |
| θ_h | 0.4π | 0.37241π | 0.39998π |
| θ_c | 0.25π | 0.22760π | 0.24969π |
| Yorktown | Theory | without M^{-1} | with M^{-1} |
| θ_e | 0.25π | 0.254793π | 0.25079π |
| θ_h | 0.4π | 0.38995π | 0.401596π |
| θ_c | 0.25π | 0.24878π | 0.25010π |

Table I. To illustrate the validity of the M^{-1} detector error compensation we show measurements of the initial condition angles with and without the M^{-1} correction. The results indicate that M^{-1} works very well.

of 8k shots as a single data point of the quantity $V = \Delta \langle B^\alpha \rangle$. Since we have $N = 20$ executions, V has 20 data points. For the variance we use the standard estimator $\sigma^2 = \frac{1}{N-1} \sum_{i=1}^N (V_i - \frac{1}{N} \sum_{i=1}^N V_i)^2$. The width of the black line in Figs. 1 and 4 stands for a 99% confidence interval which is given by $2 \times 2.576 * \sigma / \sqrt{N}$.

APPENDIX III - INHERENT HEAT LEAK DETECTION LIMITATION IN RESOURCE THEORY

Let us consider the case where the measured subsystem is the hot qubit and the parameter are $\theta_e = \theta_c \neq \theta_h$ (as in the original experiment). Moreover, we make the additional assumption that the interaction with 'e' is energy conserving so that $\Delta \langle H_e \rangle + \Delta \langle H_c + H_h \rangle = 0$. Under these condition qubit 'h' experiences a fully legitimate thermal operation. To see this, we think of 'e' and 'c' as a single object with temperature β_c . Since it holds that $\Delta \langle H_e + H_c \rangle + \Delta \langle H_h \rangle = 0$ and also 'h' is initially uncorrelated to 'c' and 'e', it follows that the dynamics is a thermal operation and therefore all the resource theory inequalities will be automatically satisfied. We conclude that in this particular scenario there is no hope of detecting heat leaks using resource theory. In some sense this is the price of using a reduced description of part of the system. Yet, in other cases, the use of reduced description can greatly simplify the quantities that have to be measured.

APPENDIX IV - THE PASSIVITY DEFORMATION PREDICTION

The passivity deformation framework [24] allows to generate new inequalities from the basic global passivity inequality

$$\Delta \langle B \rangle \geq 0$$

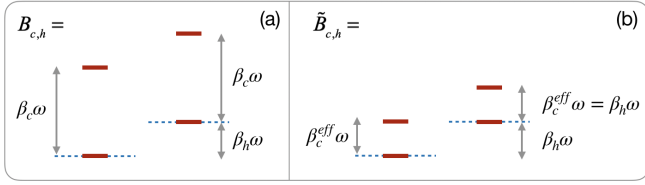


Figure 5. (a) a graphical representation of the globally passive operator B in the c-h system ($\omega = 1$ is the energy gap of the qubits). (b) By using the passivity deformation rules we lower the third and forth level by equal amounts until a level crossing is reached. This happens when $\beta_c^{eff} \omega = \beta_h \omega$. The resulting operator is guaranteed to be globally passive and it reads $\tilde{B} = \beta_h(H_c + H_h)$.

In particular, the graphic form of this framework provides a lot of insight. Let us consider the operator B (2), that corresponds to the c-h setup: $B_{c,h} = (\beta_c h_c) \otimes I_2 + I_2 \otimes (\beta_h h_h) \equiv \beta_c H_c + \beta_h H_h$ where $h_c = h_h = (\sigma_z + I_2/2)$. The additional $I_2/2$ shifts are used for making $B_{c,h}$ a positive operator. In the graphical representation of passivity deformation, we start by plotting the levels of B using “stairs” and “ladders” [24]. This plot helps to keep track of the meaning of each level. We chose one of the objects (‘c’ or ‘h’) to be the stairs and the other will be the ladder. Let us choose the cold bath to be the stairs (this choice makes no difference). We plot the levels of $\beta_c h_c$ where higher levels are shifted more to the right, which creates the dashed-line staircase shown in Fig. 5a (here there are just two levels). Next, on each floor of the staircase, we plot a “ladder” of the $\beta_h h_h$ levels (red lines). The red positioned ladders are the levels of the operator $B_{c,h}$.

Passivity deformation asserts that in order to construct new operators \tilde{B} that satisfy $\Delta \langle \tilde{B} \rangle \geq 0$ for any mixture of unitaries (3), we can use the following passivity deformation rules:

- 1) One can move levels of B up and down as long as they do not cross other levels (whether from the same ladder or from other ladders).
- 2) If levels are initially degenerate it is allowed to split them.

At the end of the deformation, we read off the resulting operator \tilde{B} and it is guaranteed to satisfy $\Delta \langle \tilde{B} \rangle \geq 0$ for any mixture of unitaries (3). Note that this deformation is just a theoretical tool for constructing new inequalities. We do not change anything in the real system. In our example we move down the third and forth levels by decreasing β_c . Eventually, to avoid level crossing (the first rule above) we have to stop when $\beta_c^{eff} \omega = \beta_h \omega$ as shown in Fig. 5b. By reading off the inequality (and for this the sideways shift is crucial) we get $\tilde{B} = \beta_h(H_c + H_h)$ (the β_h can be dropped) which is the passivity deformation operator we have used in the paper.

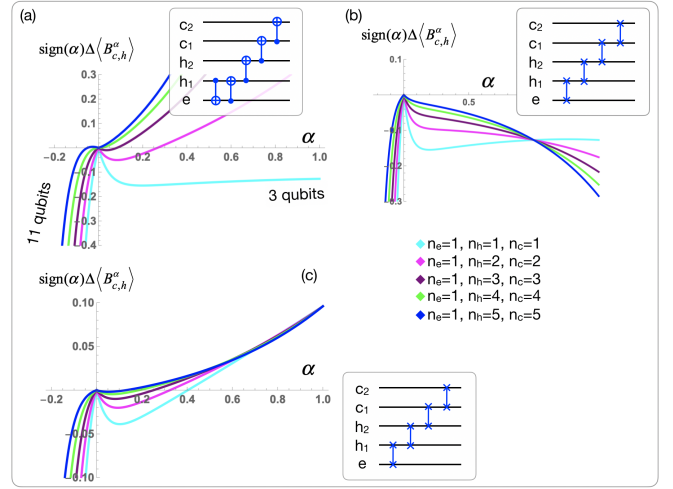


Figure 6. Numerical tests of global passivity heat leak detection in larger setups. (a) While the $0 < \alpha < 1$ detection is degraded with the system size, the $\alpha < 0$ regime keeps detecting the heat leak. In all the examples the environment is a single qubit. (b) For the same initial condition as in (a) the SWAP-based circuit in (b) shown detection for all α . Hence in (c) we change the initial condition to make the detection more difficult and once again the degradation at $0 < \alpha < 1$ occurs, yet consistent detection for $\alpha < 0$ is still observed.

APPENDIX V - HEAT LEAK DETECTION IN LARGER SETUPS

In this appendix, we numerically demonstrate that the global passivity detection capability holds also for larger setups (we simulate up to 11 qubits). In the first example of larger setups we increase the number of qubits in the hot and cold subsystems from one to 2,3,4 & 5 each. The environment, however, remains one qubit in size. Due to the asymmetry between the scaling of the environment and the system, heat leak detection becomes more difficult. The first circuit we study (inset of Fig. 6a) is the natural extension of the circuit in Fig. 2b. To illustrate an interesting behavior of the second law as the system size increases, we choose the parameter $\theta_e = 0.05\pi$, and $\theta_h = 0.4\pi$, $\theta_c = 0.25\pi$. In this case, for $n_e = n_c = n_h = 1$ the heat leak is detectable for $\alpha = 1$ (the cyan curve is negative at $\alpha = 1$). However, as the system size increases (but the environment remains one qubit) we observe that the second law can no longer detect the heat leak. In contrast, there are some value of α , in particular the negative ones, where global passivity can still quite clearly detect the heat leak.

To see if the behavior above is unique to this circuit or not, we also study the swap circuit shown in the inset of Fig 6b. As depicted in Fig. 6b for the original initial condition $\{\theta_e, \theta_h, \theta_c\} = \{0.25\pi, 0.4\pi, 0.25\pi\}$ it appear that the second law ($\alpha = 1$) successfully detects the heat leak for all the tested system sizes. Hence, there is no motivation to look at other α values. To make the

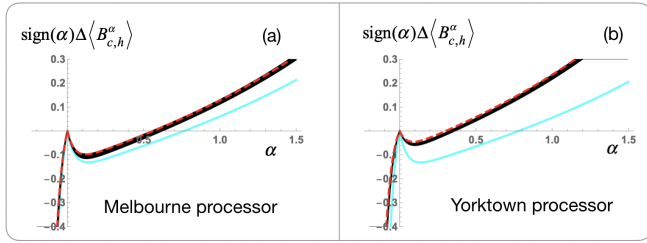


Figure 7. Reproduction of Fig. (a) with the Melbourne (a) and Yorktown (b) IBM quantum processors. The good agreement between theory (red: with unitary calibration, cyan: ideal circuit without calibration) and experiment (black) is retained, and the heat leak is detected in these two processors as well. Yet the quantitative results are not processor-independent due to the processor specific gate errors.

detection more challenging we increase θ_e (for $\theta_e = 0.5\pi$ the reduced dynamics of the c-h system becomes unital and no global passivity inequality can detect it). In Fig. 6c we change θ_e to 0.35π and observe that the second law can no longer detect the heat leak for any of the tested systems sizes. Yet the global passivity inequalities

easily detect the heat leak even in this more challenging scenario.

In summary, despite the strong circuit dependence of detection based on the second law, it appears that the negative α global passivity inequalities provide consistent detection even when the system size increases.

APPENDIX VI - USING OTHER QUANTUM PROCESSORS

To verify that the presented results are not restricted to the specific hardware of the IBM Tenerife processor we re-plot Fig. 1a using the Melbourne 14-qubit processor (Fig. 7a) and the Yorktown 5-qubit processor (Fig. 7b). The cyan line that corresponds to the ideal circuit is processor-independent. However the experimental black line differ from one processor to the other due to the different nature of the gate-errors. This is seen by the fact that we use different unitary calibration (see Sec. IID) for each processor.